The Influence of Slope Breaks on Lava Flow Surface Disruption

Lori S. Glaze, Goddard Space Flight Center, Greenbelt, MD, USA

Stephen M. Baloga, Proxemy Research, Gaithersburg, MD, USA

Sarah A. Fagents and Robert Wright, HIGP, University of Hawaii, Honolulu, HI, USA

Corresponding author: L. S. Glaze, NASA Goddard Space Flight Center, Code 690, 8800 Greenbelt Road, Greenbelt, MD 20771 (Lori.S.Glaze@nasa.gov)

Key points

- Basic models are developed for active lava flow surface disruption at a slope break
- Surface disruption can significantly affect core cooling and flow length, depth and advance rate
- Disruption length scales depend on flow regime (laminar vs turbulent) beyond slope break

Abstract Changes in the underlying slope of a lava flow impart a significant fraction of rotational energy beyond the slope break. The eddies, circulation and vortices caused by this rotational energy can disrupt the flow surface, having a significant impact on heat loss and thus the distance the flow can travel. A basic mechanics model is used to compute the rotational energy caused by a slope change. The gain in rotational energy is deposited into an eddy of radius R whose energy is dissipated as it travels downstream. A model of eddy friction with the ambient lava is used to compute the time-rate of energy dissipation. The key parameter of the dissipation rate is shown to be $\rho R^2/\mu$, where ρ is the lava density and μ is the viscosity, which can vary by orders of magnitude for different flows. The potential spatial disruption of the lava flow surface is investigated by introducing steady-state models for the main flow beyond the steepening slope break. One model applies to slow-moving flows with both gravity and pressure as the driving forces. The other model applies to fast-moving, low-viscosity, turbulent flows. These models provide the flow velocity that establishes the downstream transport distance of disrupting eddies before they dissipate. The potential influence of slope breaks is discussed in connection with field studies of lava flows from the 1801 Hualalai and 1823 Keaiwa Kilauea, Hawaii, and 2004 Etna eruptions.

Index terms 8425 Effusive volcanism

8414 Eruption mechanisms and flow emplacement

8485 Remote sensing of volcanoes

1. Introduction

When a flow changes direction, the momentum vector of the flow also changes direction. This results in the production of angular momentum when the flow transits a break in slope or is directed laterally by confining topography. Under relatively steady eruption conditions, a viscous lava flow rapidly forms a solid crust that insulates the interior of the flow. If undisturbed, this crust preserves the mobility of the hot lava core and allows the flow to travel substantial distances until the lava supply ceases or the interior of the flow cools enough to inhibit further advance. A comprehensive review of the influence of cooling, crust formation and effusion rate is contained in *Harris and Rowland* [2009].

The angular momentum generated by slope breaks and lateral confinements results in some form of circulation, eddying or vortex formation within the flow or at its margins. Pulses in lava supply can also induce circulation in the flow. When such flow patterns disturb the cooler or crusted surface of the flow, they can have a profound influence on radiative heat loss, viscosity, incipient crystallization and thus the distance a flow travels [*Finch and Macdonald*, 1953; *Booth and Self*, 1973; *Moore*, 1987; *Rowland and Walker,* 1990; *Crisp and Baloga,* 1990a, b; *Crisp and Baloga,* 1994; *Harris and Rowland*, 2001].

The only predictive attempt at calculating the extent of surface disruption appears in *Harris and Rowland* [2001]. It is based on empirical studies of core exposure as a function of flow velocities in channels and they pointed out that this dependence lacked rigorous quantification [*Harris and Rowland,* 2001, p.28]. Field measurements and theoretical modeling of the main flow from the well-documented 1984 Mauna Loa eruption show a marked increase in viscosity 5 km downstream of a major slope break at 10 km along the flow path [*Moore*, 1987; *Harris and Rowland* [2001]. With the slope embedded in the computation of flow velocity, the FLOWGO

model of *Harris and Rowland* [2001] predicts such an increase [see Figure 5 in *Harris and Rowland*, 2001] and motivates further study of slope changes and surface disruption.

There have now been more than two decades of remote sensing observations of active lava flows in numerous settings. Such images commonly show relatively broad spikes in spectral radiance (and derived metrics such as radiant flux) along the flow path that are indicative of transient or persistent disruptions of the cooler flow surface and a consequent exposure of the hotter inner core [*James et al.*, 2007; *James et al.*, 2010]. *Wright and Flynn* [2003] and *Wright et al*. [2010] give methods for estimating the core exposure of active flows from high resolution satellite remote sensing data. Although such data show indications of potential relationships between slope changes and the disruption of the lava surface, higher spatial resolution remote sensing data are needed to definitively identify a cause and effect relationship, and to place observational constraints on the length scales of disruption.

The work presented here attempts to predict the extent of flow surface disruption and core exposure due to a sudden change in the underlying slope. The model is a combination of three first-order models for different aspects of the problem. A basic mechanics model is used to approximate the rotational energy caused by a steepening slope change. Similar energy considerations apply to a shallowing slope change, lateral redirection of the flow by topographic confinements, channel constrictions and wall effects, breaches, and pulses in the lava supply rate; the resultant impact of each case on the surface disruption may be different. The gain in rotational energy is deposited into an eddy whose energy dissipates as it is transported downstream by the main flow. An elementary model of the friction between the eddy and the ambient lava provides the rate of energy dissipation as a function of time. The downstream spatial disruption of the flow surface is subsequently determined with steady-state models for the

main flow beyond the slope break: one for slow-moving flows driven by both gravity and pressure, and another for low-viscosity turbulent flows. Both models of the main flow include a volume conservation requirement at all points along the path of the flow.

The influence of surface disruption on cooling of the lava core is investigated. Implications in the context of surface disruption are given for field studies of basaltic flows from eruptions at Mt. Etna, Sicily in 2004, and the Hualalai 1801 and 1823 Kilauea eruptions in Hawaii.

2. Model Overview

The intent of the model is to develop a first-order estimate for the distance over which the surface of a steady-state flow is disrupted by a steepening of the underlying slope from one inclined plane to another. When a surface disruption occurs, it persists for a finite time as it is transported downstream by the underlying main flow. This duration is referred to here as the 'disruption time'. The corresponding 'disruption length' is obtained from the disruption time by knowing the flow velocity. The disruption length is determined by how much rotational energy is imparted by the slope break and the assumption that this energy goes into vertical circulation within the flow. This rotational energy then dissipates with time due to friction with the ambient lava. The model assumes that disruption time is given by the dissipation time.

The model considers a vertical column of height h, width w, and length dx along the flow direction. The width and density of the flow are taken as constants. The column encounters the break in slope, then rotates to a new orientation at the beginning of the downstream segment (Figure 1). The pivot of the column is taken as the slope break and no slippage is considered. For illustration purposes, the slope of the upper reach is taken as zero and the lower reach has slope ϕ with respect to the horizontal. The assumption is made that the rotational kinetic energy

114 imparted by the slope break is determined by the amount of reorientation of the column to the
115 normal of the new slope.

116 As a flow moves downslope, there is of course a change in kinetic and potential energy. In
117 steady state on a constant slope, the kinetic energy of a column remains constant, but the energy
118 gained from the decrease in potential energy is identically dissipated by the viscous stresses and
119 is converted to heat. The disruption model presented here investigates the additional rotational
120 kinetic and potential energies above the steady state main flow values. In absolute terms the
121 energy changes at the slope break could be very small compared to the downstream steady state
122 main flow values. However, the transfer of material from the upper layers of the inner core
123 resulting from the additional rotational energy can have a significant influence on the thermal
124 balance.

125 The conservation of kinetic, potential and rotational energy is used to find the new boundary
126 conditions at the beginning of the downstream segment of the flow. The volumetric flow rate is
127 conserved throughout the upstream and downstream segments of the flow. Two cases are
128 considered for the nature of the flow on the lower slope. One considers the flow to be essentially
129 laminar with the possibility that both gravity and pressure are the driving forces. The other uses
130 a gravity-driven hydraulic model more appropriate to a turbulent lava flow. Various details of the
131 main flow models appear in the appendices.

132 The induced circulations, eddies, and vortices are modeled approximately as a rotating
133 cylinder oriented transverse to the main flow direction. Although many types of flow
134 circulations are possible, they are referred to collectively as ‘eddies’ throughout this work. The
135 model assumes that the eddies cause a surface disruption that persists essentially as long as do
136 the eddies. The eddies dissipate within the flow as they are transported downstream. In the

model, the eddies generated by the slope break are simply carried by the main flow and draw no energy from the change in downstream potential energy. The dissipation rate is computed by estimating the energy lost due to eddy circulation against a viscous ambient fluid. This lost energy is removed from the eddy as the main flow travels downstream until the energy loss accumulates to a final value. For a given eddy radius, angular velocity, and viscosity, the persistence time can thus be calculated and determines the downstream eddy propagation distance. The variables for the quantitative description of this model are given under Notation.

2.1 Mechanics at the Slope Break

In going from one slope to the other, the normal to the original upstream surface rotates through an angle $\theta(t)$ from 0 at $t = 0$ to a new position with $\theta(t_f) = \phi$. At the completion of the rotation, the column is aligned with the new normal to the downstream surface (see Figure 1). The time it takes to complete this rotation is t_f. At $t = 0$, just before rotation begins as the column encounters the slope break, the column has translational kinetic energy,

$$KE = \tfrac{1}{2} mu^2, \qquad (1)$$

where m is the mass of the column and u is the flow velocity upstream of the slope break.

Across the slope break the column is treated as a physical pendulum of length h and angular velocity ω. The center of mass of the column drops due to the rotation about the pivot point adding potential energy to the column in the amount

$$PE = \tfrac{1}{2} mgh(1-\cos\phi) , \qquad (2)$$

where g is the acceleration due to gravity. The sum of the kinetic energy and the change in potential energy goes into two quantities, rotational kinetic energy and translational kinetic energy immediately after the slope break.

Using the approximation for the moment of inertia of the column, $I = mh^2/3$, the angular acceleration is given by

$$\frac{d^2\theta}{dt^2} = \frac{3g\sin\theta(t)}{2h}, \quad \text{where } \theta(0) = 0, \quad \omega = \omega(0) = u/h \ . \tag{3}$$

The elementary solution where $\sin\theta \approx \theta$ is

$$\theta(t) = \sqrt{\frac{u^2}{6gh}}\left(e^{t/\tau} - e^{-t/\tau}\right) \le \phi \ , \text{ where } \tau = \sqrt{\frac{2h}{3g}} \ . \tag{4}$$

The initial rotational kinetic energy, KE_{rot}, at the slope break is given by

$$\begin{aligned} KE_{rot}(0) = \frac{1}{2} I\omega(0)^2 \ &= \frac{1}{2}\frac{mh^2}{3}\left(\frac{u}{h}\right)^2 \\ &= \frac{1}{6}mu^2, \qquad \text{for } h > 0 \ . \end{aligned} \tag{5}$$

Equation (5) shows that as the column begins to pivot over the slope break, the rotational energy is one-third that of the incident translational kinetic energy given by equation (1). At the

completion of the rotation about the pivot point, at $t = t_f$, the rotational kinetic energy imparted by the slope break is

$$KE_{rot}(t_f) = \frac{1}{2} I\omega(t_f)^2 = \frac{1}{2}\frac{mh^2}{3}\left(\frac{u}{2h}\right)^2 \left(e^{t_f/\tau} + e^{-t_f/\tau}\right)^2 = \frac{1}{24} mu^2 \left(e^{t_f/\tau} + e^{-t_f/\tau}\right)^2, \quad \text{for } h > 0 \,. \tag{6}$$

Across the slope break an energy balance can thus be constructed. The incoming kinetic energy from equation (1), plus the change in rotational kinetic energy from equations (5) and (6), plus the gain in potential energy from equation (2), must go into the outgoing kinetic energy of the column,

$$\frac{mu^2}{2} + \frac{I\omega(0)^2}{2} + \frac{mgh}{2}\left(1 - \cos\phi\right) - \frac{I\omega_f^2}{2} = \frac{mu_2^2}{2} \,, \tag{7}$$

where ω_f is the angular velocity of the column after it has rotated through ϕ to its new orientation. Equation (7) with flow rate conservation ($uh = u_2h_2$) can be solved to obtain the outgoing velocity, u_2, on the immediate downstream side of the slope break with the selection of the physically appropriate roots. The same type of energy balance applies when a slope shallows. The main difference would be the subsequent boundary conditions and the nature of the governing transport equation beyond the slope break. A more refined approach would investigate a continuous deformation of the column across the slope break, but that requires solution of the Navier-Stokes equation and is beyond the scope of the present work.

199 The exit value of the velocity u_2 changes very little (<0.5%) from the incident conditions for
200 slopes (<15^o) relevant to most lava flows. This is because the energy balance in equation (7)
201 predominantly puts the gains in potential energy into the rotational energy that increases with
202 slope, leaving the exit flow conditions essentially unchanged. For practical purposes, therefore,
203 these velocity changes can be ignored.

204 The absolute value of the rotational energy per kg changes substantially with the slope and
205 the incident conditions, as shown in Figure 2. The vertical axis gives the exit rotational energy
206 $KE_{rot}(t_f)$ per kg as a function of the change in underlying slope. The relative changes in the
207 rotational kinetic energy are illustrated by considering three flow depths (h = 1, 3 and 6 m; gray,
208 red, and green curves, respectively) and two incident flow velocities (u = 1 and 2 m s^{-1}; solid and
209 dashed curves, respectively). The rotational energy acquired from the slope break increases with
210 incident flow thickness and changes by factors of 2, 4, and 7 (gray, red, green curves) for the
211 thicknesses shown over slope changes up to 15˚. When the incident velocity is doubled (dashed
212 curves), there is the same dependence on flow depth and slope, but there is an additional overall
213 increase in the rotational energy, as expected. A much greater sensitivity to slope is found by
214 changing the flow depth keeping the velocity constant.

215

216 **2.2 Eddy Dissipation**

217 Eddies are produced by the angular momentum generated by the slope break. In the first-
218 order model used here, the eddy is treated as a cylinder of fluid with radius R that rotates as it is
219 transported downstream by the main flow. The best case for the persistence of an eddy is when
220 its surface is in contact only with the ambient fluid that transports it. In the worst case, an eddy
221 contacts counter-rotating neighboring eddies and breaks into smaller ones.

At time $t = t_f$, the rotation of the lava column due to the slope break is completed and an eddy is established. The time of eddy dissipation is then measured with time beginning at t_f. The rotational kinetic energy from the slope break is deposited into rotational energy of the eddy, thus

$$KE_{rot}(t_f) = \frac{1}{2} I_e \omega_{eo}^2 = \frac{1}{2}\left(\frac{1}{2} m_e R^2\right)\omega_{eo}^2 \quad , \tag{8}$$

where m_e and I_e are the mass and moment of inertia of the eddy, respectively. The initial angular velocity of the eddy rotation, ω_{eo}, can be found by re-arranging equation (8) to be

$$\omega_{eo} = \sqrt{\frac{4KE_{rot}(t_f)}{R^2 m_e}} = \frac{2}{R}\sqrt{\frac{KE_{rot}(t_f)}{m_e}} = \frac{2}{R}\sqrt{\frac{m}{m_e}\frac{KE_{rot}(t_f)}{m}} \quad , \tag{9}$$

where the rotational kinetic energy per unit mass is obtained from the energy balance for the column in equation (6).

The resistive force on the eddy due to ambient lava is approximated by

$$F = \mu A_e \frac{dv}{dr} \approx \mu A_e \omega_e(t) \quad , \tag{10}$$

where A_e is the surface area of the eddy in contact with ambient lava. Assuming the eddy retains its integrity, cumulative energy lost due to friction over time beginning with t_f is given by

$$W_{diss}(t) = \int_{t_f}^{t} F ds \approx \mu A_e \int_{t_f}^{t} \omega_e(t) ds = \mu(2\pi R w)\int_{t_f}^{t} \omega_e(t)\frac{ds}{dt} dt, \quad t \geq t_f \, . \tag{11}$$

The variable s is the distance a point on the cylinder travels to dissipate the energy W_{diss} by friction with the ambient fluid, given by

$$s(t) = R\int_{t_f}^{t} \omega_e(t)dt = R\omega_{eo}\frac{\Gamma}{4}\left(1 - e^{-4(t-t_f)/\Gamma}\right). \quad (12)$$

To determine the amount of dissipation after the onset of eddy rotation, $\omega_e(t)$ must also be determined. The time dependence for the deceleration of eddy rotation due to friction is found from Newton's 2nd law

$$I_e\frac{d\omega_e}{dt} = -FR \approx -\mu A_e \omega_e R\ . \quad (13)$$

Integrating equation (13), we obtain

$$\int_{\omega_{eo}}^{\omega_e(t)} \frac{d\omega_e}{\omega_e} = -\frac{2\mu A_e}{m_e R}\int_{t_f}^{t} dt\,, \quad (14)$$

and an expression for $\omega_e(t)$ is found to be,

$$\omega_e(t) = \omega_{eo}e^{-4(t-t_f)/\Gamma}; \quad \text{where } \Gamma = \frac{\rho R^2}{\mu}\ . \quad (15)$$

This shows that the critical parameter for eddy dissipation is the time constant Γ. It can also be expressed in terms of the Reynolds number of the flow itself, Re = $\rho u_2 h_2/\mu$ as $\Gamma = \mathrm{Re}R^2/q_o$. Fast-moving, high-Re flows will have long time constants and the effects of slope breaks will tend to propagate greater distances downstream and vice versa.

The rotational energy lost to friction is given by equation (11), using equations (12) and (15), as

$$W_{diss}(t) = \frac{m_e R^2}{4}\omega_{eo}^2\left(1 - e^{-8(t-t_f)/\Gamma}\right) = KE_{rot}(t_f)\left(1 - e^{-8(t-t_f)/\Gamma}\right), \qquad (16)$$

which yields the time decay of rotational energy due to the friction of the eddy. Curves relevant to lava flows are shown in Figure 3. Slightly more than half (55%) the initial rotational energy is dissipated by friction in 0.1 time constant, 98% is dissipated in half a time constant, and 99.99% is dissipated when t-$t_f = \Gamma$. Thus Γ is a reasonable estimate of the dissipation time and, by assumption, the disruption time.

2.3.1 Eddy Size

Many factors could influence the circulation of a flow as it traverses a change in slope or encounters a topographic barrier. These include the character of the incident flow (laminar, turbulent, or disrupted), roughness of the flow bed, the presence of entrained and incipient solids, and interactions with channel walls. All such factors require independent theoretical or empirical studies.

There is a link between the volume of the fluid column and the volume of the eddy that is the recipient of the rotational energy imparted by the slope break. To embrace a range of eddy sizes,

285 the extent of the column along the direction of flow (dx) is prescribed to be the diameter of the
286 eddy ($2R$; Figure 1). Thus the fraction of column volume that receives the rotational energy is
287 given by
288
289 $$\Im = \frac{\text{vol. eddy}}{\text{vol. col.}} = \frac{\pi}{2}\left(\frac{R}{h}\right). \qquad (17)$$
290
291 For a large circulation, R might approach $h/2$ as suggested by engineering experience with
292 turbulent flow in pipes. It is difficult to estimate a minimum relevant size of an eddy in a lava
293 flow. However, from a practical standpoint a lower limit can be estimated by considering an
294 incident laminar flow. Appendix A gives the cumulative rotational energy for an incident laminar
295 flow as it traverses the slope break. Due to the strong dependence of rotational energy on the
296 height within the flow, only 3% of the rotational energy would come from the lower half of the
297 flow and only about 11% from the lower two-thirds. The upper 5% of the flow contributes
298 almost a quarter of the rotational energy and so $R = 0.1h$ is taken as a practical minimum value
299 for eddy radius.
300 The time constants for eddy dissipation shown in Table 1 are clearly dominated by the
301 viscosity and the eddy size, which must be roughly proportional to the flow depth. Figure 3
302 shows the relative dissipation as a function of time for Γ = 100, 200, 500 and 1000 s from
303 equation (16). Low-viscosity lavas imply large time constants, and such flows are predicted to
304 maintain circulations for long times, tens of seconds or more. Eddies would be carried substantial
305 distances downstream by any fast-moving segment of the flow. If the flow is turbulent, however,
306 the simplistic model used here would require significant modification to account for the decay of

307 larger eddies into smaller ones. Conversely, high-viscosity flows could manifest the influence of
308 circulation by local cooling, stagnation, and inflation.

309 The dominant role of viscosity in determining the extent of surface disruption calls into
310 question the validity of viscosity estimates derived from field measurement of active flows.
311 Usually such estimates are derived from the Jeffreys' equation for a steady-state flow of constant
312 depth [*Nichols*, 1939], although numerous modifications have been made to account for time-
313 dependent effects [e.g., *Baloga and Pieri*, 1986], lava yield strength [e.g., *Harris and Rowland*,
314 2001], levee building [e.g., *Glaze et al*., 2009], and similar factors. These formulations do not
315 account for the fluid pressure caused by the resulting topographic gradients in the flow. It is
316 shown in Appendix B that the incorporation of seemingly small pressure gradients causes an
317 important systematic departure from the steady-state constant depth assumptions of the Jeffreys'
318 approach. The primary consequence is that evaluations of viscosity based on field measurements
319 of flow parameters could be overestimated by an order of magnitude or more in the case of thick
320 (50–200 m) flows on other planetary surfaces.

321

322 # 3. Implications

323 ## 3.1 Influence of Flow Surface Disruption on Core Temperature

324 The potential influence of surface disruption on the core temperature is illustrated by
325 considering a schematic flow of constant depth h_2 and velocity u_2 that begins with temperature T_o
326 at the top of an inclined plane. The core temperature is computed by the basic steady state
327 radiation loss formula

328

329 $$T_{core}(x) = T_o \left[1 + \frac{3 f \varepsilon \sigma T_o^3}{\rho C_p} \frac{h_2 x}{u_2} \right]^{-1/3}, \quad (18)$$

330

331 using the flow parameters given in Table 2, with f denoting the areal fraction of exposed hot lava
332 core within the crusted flow surface, and σ being the Stefan-Boltzmann constant.

333 The degree to which the disrupted upper layer of a lava flow exposes core lava depends upon
334 many factors, including the viscosity of the lava and the thickness and mechanical strength of the
335 crust. We do not attempt to draw a direct link between the rotational eddies and the ability to
336 actually "disrupt" the surface crust. However, several cases exploring a range of potential f
337 values can be explored to place bounds on the sensitivity of increased surface disruption over
338 short distances.

339 Figure 4 shows the resulting temperature profiles along the length of the flow, for three cases
340 having different values of f. The uppermost curve assumes a core exposure fraction of f = 0.05,
341 which is somewhat high for most flows [*Crisp and Baloga*, 1990a; *Oppenheimer*, 1991; *Wright*
342 *et al.*, 2000; *Wright et al.*, 2010]. For comparison, the lowermost curve uses an extreme value of
343 f = 0.5. The red curve shows the strong influence of the T^4 radiation term when the flow surface
344 is disrupted by eddies. Twelve 60 m segments of disruption with f = 0.9 were inserted in the first
345 2 km of the flow, followed by three others further downstream. Everywhere else, a value of f =
346 0.05 was applied. The disruption in the first 2 km of the flow causes a major drop (35˚C) in the
347 core temperature. Using equation (3) of *Harris and Rowland* [2001], such a temperature drop
348 would cause the core viscosity to increase by a factor of 4. This would have a significant
349 influence on the advance velocity and the depth of the flow. A few segments of surface
350 disruption upstream will have a significant impact on the ultimate flow length.

351

352 **3.2 The September 2004 Lava Flow at Mt. Etna**

353 A relatively well-documented flow-producing eruption exemplifying laminar flow (Appendix
354 B) occurred at Mt. Etna, Sicily in 2004-2005 [e.g., *Mazzarini et al.*, 2005; *Burton et al.*, 2005].
355 Comprehensive dimensional data on the flow were acquired by airborne laser altimetry
356 *Mazzarini et al.* [2005]. Analysis of 162 profiles indicated a typical flow thickness of 5 m,
357 although there is considerable variability, with a maximum of 17 m. Both *Mazzarini et al.* [2005]
358 and *Wright et al.* [2010] show that 20–30˚ slopes are common, and field observations obtained
359 from the *Global Volcanism Network* [2004] suggest that 1 m s^{-1} is a representative flow velocity.
360 The eddy dissipation relationship (Figure 3) shows that the influence of slope changes (or
361 equivalent influences) decays in ~0.5–2 min. for $\Gamma_{-}^{\sim}$ 100–200 s. With channel velocities of 1 m
362 s^{-1}, this corresponds to disruption lengths of 30–120 m. In Appendix B, it is shown that the use of
363 the Jeffreys' equation (commonly used for flow velocity calculations) can significantly
364 overestimate the viscosity of active flows, so a dissipation time on the order of hundreds of
365 seconds may be reasonable. If the lava viscosity was significantly in excess of hundreds of Pa s,
366 the dissipation time could be on the order of seconds to a few tens of seconds for eddies of ≤ 1 m
367 and a flow thickness of 5 m. However, significant slope changes occur about every 100 m along
368 the 2004 Mt. Etna flow path. Even with a relatively rapid dissipation rate, the repeated slope
369 changes at length scales comparable to the dissipation lengths keep adding flow circulation and
370 surface disruption.

371 One potentially useful approach to validating and placing constraints on the proposed model
372 is to correlate changes in lava flow surface temperature, derived from remote sensing thermal
373 imaging, with underlying surface topography and slopes. However, the spatial resolution of even

some of the best orbiting thermal imagers, such as Hyperion (30 m pixels), is insufficient. In order to distinguish changes in surface radiance on the order of the disruption scales (30 – 120 m for a flow like the 2004 Mt. Etna flow) requires spatial resolutions about an order of magnitude finer (~5-10 m pixels). One approach for future work is to use field thermal imagers that are capable of spatial resolutions on the order of 5-10 m/pixel (or better), with specific application to this problem to ensure synoptic coverage over the full length of possible disruption. Such field campaigns have successfully documented variations in lava flux [*James et al.*, 2007; *James et al.*, 2010]. In particular, *James et al.* [2007] examine the time dependent thermal flux of several lava flows during the 2004-2005 eruption at Mt. Etna that progress from a steeper to a shallower slope. A similar technique would be appropriate here for lava flowing onto a steeper slope. It is important to note that such a field campaign must adequately characterize the time dependent changes in thermal flux owing to pulses in lava flux in order to distinguish the systematic surface disruption due to the change in slope.

3.3 The 1801 Hualalai Flow, Hawaii

The possibility of turbulent lava flows has been postulated for many years [e.g., *Nichols*, 1939, p.294; *Shaw and Swanson*, 1970; *McGetchin and Eichelberger,* 1975; *Baloga et al.*, 1995]. Turbulence can be caused not only by high flow velocities and low viscosities, but also constrictions and widenings of the flow, small and large-scale topographic variations, and the motions of entrained crystals and ambient materials. Although there is some disagreement on the eruption rates during the 1801 Hualalai lava flow [*Kauahikaua et al.*, 2002], with viscosity determined by petrologic studies to lie in the range 10^1–10^2 Pa s, and field estimates of flow velocities of ~10 m s^{-1}, the 1801 Hualalai eruption likely produced at least transient turbulent

lava flows with depths of ~5 m near the source. The uncommonly deep (6–18 m) downstream channels may have formed in part through construction due to very short duration overflow events, however, even partially full, greater turbulence through these stretches is expected [*McGetchin and Eichelberger,* 1975; *Guest et al.,* 1995].

The 1801 Hualalai flow also traversed several large changes in slope (3–6˚) along the flow path [*Baloga et al*., 1995]. Xenoliths were deposited as bedload at the beginning of the final reach toward the ocean. From that point, the decay of these circulations and intense cooling produced a morphology common to other basaltic channelized flows on low slopes.

The elementary turbulent flow model in Appendix B indicates that such a flow would reach the terminal velocity on a flat plane in tens to ~100 m from the source or slope break. Using the range of likely terminal velocities (5–15 m s^{-1}) suggested in *Baloga et al.* [1995], the computed disruption lengths are shown in Figure 5 for appropriate Hualalai parameters (ρ = 2600 kg m^{-3}, h = 5 m, R_1 = 1 m, ϕ = 10˚) and viscosities of 50–500 Pa s spanning the range identified by *McGetchin and Eichelberger* [1975]. With the eddy radius taken as only 20% of the flow depth, the computed flow disruptions extend for hundreds of meters to a kilometer or so. The circulations gained from the slope breaks most likely contributed significantly to the suspension of the xenoliths. Given that there are several slope breaks along the flow, such disruption lengths are consistent with the complex morphologic features of the flow [*McGetchin and Eichelberger,* 1975; *Baloga et al.,* 1995; *Guest et al.,* 1995] until the very shallow slopes near the ocean.

3.4 The 1823 Keaiwa “Great Crack” Flow, Kilauea Volcano, Hawaii

The 1823 Keaiwa flow from the Great Crack fissure at Kilauea also produced rapidly moving low-viscosity flows. Near the source *Guest et al.* [1995] estimated the velocity at 15 m s^{-1}. Field

420 evidence suggests a source depth of <0.5 m with a downstream thickening in distal regions to
421 only 1–2 m near the ocean [*Guest et al.,* 1995; *Baloga et al*., 1995; and sources cited therein].
422 The predominant underlying slope is about 5˚ from the fissure to the ocean (a distance of ~4 km
423 using Area 2 of Figure 4 from *Baloga et al*. [1995]). The flow apparently issued from the Great
424 Crack as a rapidly moving sheet, transitioning to a slabby 'a'a at the distal margins. The
425 turbulent main flow model (Appendix B), using the parameters $u(0)$ = 15 m s^{-1}, $h(0)$ = 0.5 m, ϕ_2
426 = 5˚ and h_2^* = 2 m, indicates that the flow would attain a velocity u_2 of 3.75 m s^{-1} in ~100 m.
427 Thus, the 4 km transit time to the ocean would be ~1000 s. The model used in *Baloga et al*.
428 [1995] assumed a constant velocity of 10 m s^{-1} from the fissure to the ocean resulting in a transit
429 time about half this value. With a velocity of 3.75 m s^{-1}, $R \approx$ 0.5–1 m and μ = 100 Pa s, Table 1
430 suggests a disruption length of about 24–98 m. Due to the thinness of the flow, small-scale
431 topographic variations could occur over such a disruption length, feeding the slope induced
432 circulations. The resulting mixing would have contributed to the homogeneity of the advancing
433 sheet, but the transit time was evidently too short to permit a significant increase in the viscosity.
434

435 ## 4. Summary and Conclusions

436 Changes in slope or the lateral redirection of a lava flow impart a significant fraction of the
437 incident kinetic energy of the flow into rotational energy. For steepening slopes, the eddies,
438 circulation and vortices caused by this rotational energy can disrupt the flow surface and have a
439 significant impact on the heat loss and thus the distance the flow can travel. The quantity of
440 rotational energy imparted to the downstream flow is more sensitive to the flow depth than the
441 incident flow velocity. There is a relatively large quantity of potential energy available from the
442 main flow compared to the rotational energy of eddies that disrupt the surface and alter the

443 thermal balance. The preliminary model presented in this work does not draw energy from the
444 main flow. Repeated slope changes and rough topography could significantly extend the
445 disruption of the flow surface. Many lava flows experience multiple slope breaks of various
446 magnitudes that can combine to disrupt the surface. A more refined theoretical treatment and
447 comprehensive field measurements are needed to explore this possibility.

448 This work provides only a first-order analysis of the essential steps in disrupting a lava flow
449 surface to the extent that it could affect the thermal heat balance of the flow. Consequently, there
450 are numerous opportunities for improvement at each step of the analysis. First, in transitioning an
451 abrupt slope break, a continuum approach based on Navier-Stokes equations would provide a
452 refinement. Relaxing the assumption of an abrupt slope change is also a more realistic approach.

453 The physics of eddy dissipation is another area for future study. Circulations, particularly if
454 turbulence is generated, are three-dimensional, unlike the planar assumptions used here. This
455 suggests that a horizontal component of rotation and dissipation must also be included. Lateral
456 confinements, wall effects, and changes in the lateral direction of the flow path could contribute
457 significantly to the rotational energy of the flow and thus to surface disruption. Unlike the simple
458 estimate used here, the physical sizes of the eddies diminishes as they propagate downstream.
459 The details of how these considerations affect the heat balance are reserved for a future study.
460 Nonetheless, such improvements in the theory might provide a basis for future field studies and
461 approaches to flow and eruption dynamics inferred by remote sensing.

462 Besides the parameters of the incident flow, this work shows that the primary factors
463 controlling the surface disruption are the size of the eddies and the viscosity of the downstream
464 ambient lava. The model results obtained in this work are at least qualitatively consistent with
465 surface disruptions interpreted for the fast-moving flows from the 1801 Hualalai and 1823

Keaiwa eruptions, as well as a recent flow at Mt. Etna. Future avenues for developing model constraints include comparison of predicted disruption lengths with high spatial resolution thermal remote sensing data. Future modeling work will include investigation of other likely contributors to circulations and surface disruption in active lava flows.

Appendix A: Cumulative Rotational Kinetic Energy

Here the cumulative rotational kinetic energy of the column in laminar flow as it encounters an abrupt slope break is calculated. Within the flow, the velocity profile is taken as

$$u(z) = \frac{\rho g \sin\theta_1}{\mu} z\left(h_1 - \frac{z}{2}\right), \qquad \text{(A1)}$$

where h_1 is an arbitrary height within the flow interior up to the top surface at h. The upstream surface is assumed to be inclined to the horizontal at an angle θ_1. If there is no inclination of the upper surface, the flow is driven by a constant pressure (momentum flux) and the calculation procedes replacing $g\sin\theta_1$ with gdh/dx

The rotational kinetic energy up to h_1 is

$$KE_{rot}(h_1) = \frac{I(h_1)\omega(h_1)^2}{2} = \frac{1}{2}\frac{\rho h_1^3 w dx}{3}\left(\frac{u(h_1)}{h_1}\right)^2 = \frac{1}{2}\frac{\rho h_1^3 w dx}{3}\left(\frac{g\sin\theta_1 h_1^2}{2\nu h_1}\right)^2 = \frac{1}{24}\frac{\rho g^2 (\sin\theta_1)^2 h_1^5 w dx}{\nu^2}, \qquad \text{(A2)}$$

where, ν is the lava kinematic viscosity (= μ/ρ). Note that the moment of inertia and the angular velocity depend on h_1 and the strong dependence on the flow depth. Up to the full height h of the flow we have:

$$KE_{rot}(h_h) = \frac{1}{24}\frac{\rho g^2 (\sin\theta_1)^2 h^5 w dx}{\nu^2} \quad . \qquad \text{(A3)}$$

Thus the cumulative rotational KE fraction as a function of h_1 is

$$r = \frac{KE(h_1)}{KE(h)} = \left(\frac{h_1}{h}\right)^5 . \qquad \text{(A4)}$$

This shows, as expected, that the very upper layers of a laminar flow contribute the vast majority of rotational kinetic energy as the flow goes over an abrupt slope break (see Figure A1).

Appendix B: Main Flow Transport

The main flow modeling referred to in the text is presented below. The analysis of the mechanics of the slope break provides the boundary conditions for main flow transport of the eddies beyond the slope break. The depth and velocity of the main flow may change as a function of distance beyond the slope break, but the volumetric flow rate is conserved at all locations downstream.

The laminar case

506 The governing equation for the flow depth is taken as

507

508 $$\frac{\partial h_2}{\partial t} + \frac{g \sin\phi h_2^2}{\nu} \frac{\partial h_2}{\partial x} = \frac{g \cos\phi}{3\nu} \frac{\partial}{\partial x}\left(h_2^3 \frac{\partial h_2}{\partial x} \right) \quad , \qquad \text{(B1)}$$

509

510 where ν is the kinematic viscosity of the lava (= μ/ρ). The second term on the left-hand side
511 represents gravity as a driving force while the right-hand side represents the influence of fluid
512 pressure. The pressure term is often ignored in volcanologic applications, but is a critical term in
513 hydraulic formulations. Here we consider the steady-state solution of equation (B1). The first
514 integration gives

515

516 $$q_o = u_2(0) h_2(0) = \left(\frac{g \sin\phi h_2^3}{3\nu} - \frac{g \cos\phi}{3\nu} h_2^3 \frac{dh_2}{dx} \right) = u_2(x) h_2(x) \quad , \qquad \text{(B2)}$$

517

518 where q_o is the volumetric flow rate per unit flow width. A more convenient form is given by,

519

520 $$1 = \left(\frac{h_2}{h_J} \right)^3 \left(1 - \cot\phi_2 \frac{dh_2}{dx} \right) \qquad h_J = \sqrt[3]{\frac{3 q_o \nu}{g \sin\phi_2}} \quad . \qquad \text{(B3)}$$

521

522 where h_J is the oft-cited Jeffreys' steady-state flow depth.

523 Three types of possible behaviors are evident from equation (B3), depending on the boundary
524 conditions ($u_2(0)$, $h_2(0)$), the slope, and the viscosity. The different modes of flow behavior are

associated with three roots of equation (B2) or (B3). The critical value that determines the behavior of the flow is the Jeffreys' flow depth h_J.

What is remarkable about the inclusion of pressure in the steady state is that the Jeffreys' steady-state flow depth can only be attained for one fortuitous set of conditions of flow rate, slope, and viscosity and boundary conditions ($u_2(0)$, $h_2(0)$). For $h_2 < h_J$ ($u_2 > u_J$,) the flow must thin and accelerate as it moves from $x = 0$. In steady state, the flow regime actually moves further away from Jeffreys' conditions with distance from the source until the steady-state assumption is no longer valid, the viscosity increases due to cooling, or a traveling wave is established [*Mei*, 1966].

For $h_2 > h_J$, the flow must thicken and slow. In this case, the pressure term will always attempt to drive the flow toward a pond-like topography with $dh_2/dx \approx \sin\phi_2$. This has nothing to do with whether there is a slope break upstream, it is solely a function of the driving forces. The regimes associated with equation (B3) are clearly analogous to supercritical and subcritical hydraulics concepts. The tendency to produce an almost horizontal upper surface topography on shallow slopes may be one of the principal factors causing pahoehoe lobe inflation [*Hon et al*., 1994; *Keszthelyi et al*., 1999; *Glaze and Baloga,* 2013].

The analytic solution of equation (B3) is found by changing variables and the boundary condition

$$\psi(\xi(x)) = h_2(\mathrm{x}) / h_J, \quad \xi(x) = \tan\phi_2 x / h_J$$
$$\psi(0) = h_2(0) / h_J, \quad \xi(0) = 0 \qquad \text{(B4)}$$

With these changes, the solution of equation (B3) requires integration of

547

548 $$\int \frac{\psi^3 d\psi}{\psi^3 - 1} = \xi \ . \qquad \text{(B5)}$$

549

550 The key to the integration of equation (B5) is the expansion of the denominator in terms of the
551 real and two conjugate roots and the subsequent use of partial fraction expansions.

552

553 $$\int \frac{\psi^3 d\psi}{\psi^3 - 1} = \int \left[\left(\psi - 1\right)\left(\psi + \frac{1}{2} + \frac{i\sqrt{3}}{2}\right)\left(\psi + \frac{1}{2} - \frac{i\sqrt{3}}{2}\right) \right]^{-1} \psi^3 \, d\psi \ , \qquad \text{(B6)}$$

554

555 where $i=\sqrt{(-1)}$. With the use of the partial fraction expansions and considerable algebra, we find

556

557 $$\int \frac{\psi^3 dz}{\psi^3 - 1} = \psi + \ln(\psi - 1)^{1/3} + \frac{\sqrt{3}}{3}\tan^{-1}\left(\frac{\sqrt{3}}{1 + 2\psi}\right) - \ln(\psi^2 + \psi + 1)^{1/6} . \qquad \text{(B7)}$$

558

559 Thus the solution of equation (B3) in the ψ variable is

560

561 $$\xi = \psi - \psi(0) + \ln\left(\frac{\psi - 1}{\psi(0) - 1}\right)^{1/3} + \frac{\sqrt{3}}{3}\tan^{-1}\left(\frac{\sqrt{3}}{1 + 2\psi}\right) - \frac{\sqrt{3}}{3}\tan^{-1}\left(\frac{\sqrt{3}}{1 + 2\psi(0)}\right) - \ln\left(\frac{\psi^2 + \psi + 1}{\psi(0)^2 + \psi(0) + 1}\right)^{1/6}$$

562

563 The analytic solution is found by undoing the change of variables from ψ back to h using
564 equation (B4). The analytic solution then gives the longitudinal flow profile $h(x)$. Because the
565 flow rate is constant along the flow path, equation (B2) then provides $u(x)$.

Figure B1 illustrates the dramatic influence of pressure on the longitudinal thickness profiles compared to a constant Jeffreys solution, for a flow rate and viscosity and slope that give $h_J = 5$ m. For clarity of illustration, the slope is taken as 0.2°. Once the flow rate, slope and viscosity are fixed, small increases in the flow depth at the source cause a significant departure from the constant Jeffreys' flow depth. The most important consequence of this analysis is that field estimates using Jeffreys' equation can significantly overestimate the viscosity. Figure B1 shows that at 3–4 km from the source, the flow has more than doubled beyond h_J. Because viscosity estimates go as h^3, the viscosity estimate would be overestimated by at least an order of magnitude. This sensitivity suggests that field measurements should measure the topographic gradient as well as the flow depth as is commonly done in hydrologic applications.

The turbulent case

Under conditions of turbulent flow, following the formalism of basic hydraulics, the re-oriented column on the lower reach (see Figure 1) experiences only two forces, gravity and flow bed resistance characterized by a single parameter, the bed stress. Consistent with a first-order analysis, the governing equation is taken as

$$m\frac{du_2}{dt} = mg\sin\phi - \sigma_b A \ , \qquad \text{(B8)}$$

where σ_b is the stress at the flow bed and A is the area of bed contact with the flow.

The common hydraulic application of this formulation is to empirically relate the bed stress under many different types of ambient conditions (e.g., bed roughness, channel geometry) to an

588 equilibrium flow depth. Similarly, a prescribed value of h_2^* is used here. With such an
589 assumption, and the conservation of flow rate, equation (B8) reduces to
590
591 $$u_2 \frac{du_2}{dx} = g \sin\phi \left(1 - \frac{h_2^*}{h_2}\right) = g \sin\phi \left(1 - \frac{h_2^* u_2}{q_o}\right), \quad \text{with } q_o = h_2(0)\,\mathrm{u}_2(0) \ . \quad \text{(B9)}$$
592
593 The velocity is given by
594
595 $$u(0) - u_2 - \frac{1}{\alpha} \ln\left(\frac{1 - \alpha u_2}{1 - \alpha u(0)}\right) = \alpha g \sin\phi x, \quad \text{with } \alpha = h_2^* / q_o \ . \quad \text{(B10)}$$
596
597 This solution in general also has two regimes of flow behavior, but they approach the
598 equilibrium flow depth h_2^* from above and below this depth. As the flow depth changes with
599 distance, there are corresponding changes in the flow velocity to keep the flow rate constant. The
600 simple model above assumes the flow is planar (i.e., infinitely wide), unlike actual flows with
601 lateral confinement. Recent advances in hydraulic engineering show how to extend this
602 elementary formulation to account for secondary flows within the main flow and the influence of
603 narrow and wide stress-inducing lateral boundaries [*Guo and Julien*, 2005].
604
605 **Notation**
606 A area of contact between turbulent flow and flow bed (constant), m^2
607 A_e area of contact between eddy and ambient lava (constant), m^2
608 C_p specific heat capacity of lava, J kg^{-1} K^{-1}
609 dx length of column in direction of incident flow (variable), m

610	f	fraction of exposed lava core
611	F	resistive force acting on eddy, N
612	g	acceleration due to gravity, m s^{-2}
613	h	depth of the incident flow (constant), height of column entering slope break, m
614	h_2^*	equilibrium turbulent flow depth on lower surface (constant), m
615	h_2	flow depth on lower (2^{nd}) surface (space dependent), m
616	$h_2(0)$	flow depth on lower (2^{nd}) surface after column rotation (constant), m
617	h_J	Jeffreys' steady-state flow depth, m
618	I	moment of inertia of column (constant), kg m^2
619	I_e	moment of inertia of eddy (constant), kg m^2
620	KE	translational kinetic energy of the incident flow (constant), J
621	$KE_{rot}(0)$	initial rotational kinetic energy of the incident flow (constant), J
622	m	mass of the column (constant), kg
623	m_e	mass of eddy (constant), kg
624	PE	potential energy gained by column rotation (variable), J
625	q_o	lava volume flow rate per unit channel width, m^2 s^{-1}
626	r	cumulative rotational kinetic energy fraction for laminar flow
627	R	radius of circulating eddy (constant), m
628	s	distance on the eddy through which the resistive force F acts (time dependent), m
629	t	time, s
630	t_f	time required to rotate column through an angle ϕ (variable), s
631	T_o	initial lava core temperature (K)
632	T_{core}	temperature of lava core (K)
633	u	velocity of the incident flow (constant), m s^{-1}
634	u_2	flow velocity on lower (2^{nd}) surface (space dependent), m s^{-1}
635	$u_2(0)$	flow velocity on lower (2^{nd}) surface after column rotation (constant), m s^{-1}
636	w	width of flow (constant), m

W_{diss}	energy lost from eddy due to friction with ambient lava (time dependent)
Γ	time constant for eddy dissipation (constant), s
ε	lava emissivity
θ	angle through which column rotates (time dependent)
μ	dynamic viscosity of lava (constant), Pa s
ν	kinematic, viscosity of lava (constant), $m^2\ s^{-1}$
ρ	lava density
σ	Stefan-Boltzmann constant, $5.670373(21)\times10^{-8}$ W m^{-2} K^{-4}
C_p	specific heat of lava
T	lava core temperature
σ_b	bed stress for resistance to turbulent flow (constant)
τ	time constant for angular rotation of column (constant), s
ϕ	slope of the flow bed after the slope break (constant)
ω	angular velocity of column (time-dependent)
ω_e	angular velocity of eddy rotation (time-dependent)
ω_{eo}	initial angular velocity of eddy rotation (constant)
ω_f	angular velocity of column after it has rotated through angle ϕ (constant)
$\Im$	ratio of eddy volume to column volume

Acknowledgments. Work performed by SMB and LSG was sponsored by NASA grants NNX10AP63G and NNXAR10G. LSG also acknowledges partial support from the NASA Planetary Geology and Geophysics program (WBS 811073.02.01.05.80).

References

Baloga, S., and D. Pieri (1986), Time dependent profiles of lava flows*, J. Geophys. Res., 91,* 9543–9552.

Baloga, S. M., P. D. Spudis, and J. E. Guest (1995), The dynamics of rapidly emplaced terrestrial lava flows and implications for planetary lava flows, *J. Geophys. Res.*, *100*, 24,509–24,519.

665 Booth, B., and S. Self (1973), Rheological features of the 1971 Mt Etna lavas, *Proc. Roy. Soc.*
666 *Lond., Ser. A*, 274, 99–106.

667 Burton, M. R., et al. (2005), Etna 2004-2005: An archetype for geodynamically-controlled
668 effusive eruptions, *Geophys. Res. Lett*., *32,* L09303 doi:10.1029/2005GL022527.

669 Crisp, J. A., and S. M. Baloga (1990a), A model for lava flows with two thermal components, *J.*
670 *Geophys. Res.*, *95*, 1255–1270.

671 Crisp, J. A., and S. M. Baloga (1990b), Methods for estimating eruption rates of planetary lava
672 flows, *Icarus*, *85*, 512–515.

673 Crisp, J. A., and S. M. Baloga (1994), Influence of crystallization and entrainment of cooler
674 material on the emplacement of basaltic aa lava flows, *J. Geophys. Res.*, *99,* 11,819–11,831.

675 Finch, R. H., and G. A. Macdonald (1953) Hawaiian volcanoes during 1950, *U.S. Geol. Surv.*
676 *Bull., 996-B*, 89pp.

677 Glaze, L., S. M. Baloga, W.B . Garry, S. A. Fagents, and C. Parcheta (2009), A hybrid model for
678 leveed lava flows: Implications for eruption styles on Mars, *J Geophys Res*, *114,* E07001, doi:
679 10.1029/2008je003278.

680 Glaze, L. S., and S. M. Baloga (2013), Simulation of inflated pahoehoe lava flows, *J. Volcanol.*
681 *Geotherm. Res., 255*, 108–-123

682 Global Volcanism Network (2004), Mt. Etna, *Bull. Global Volc. Network, 29*(4), Smithson. Inst.,
683 Wash. D.C.

684 Guest J., P. Spudis, R. Greeley, G. J. Taylor, and S. M. Baloga (1995), Emplacement of xenolith
685 nodules in the Kaupulehu lava flow, Hualalai volcano, Hawaii, *Bull. Volcanol., 57*, 117–126.

686 Guo, J., and P. Y. Julien (2005), Shear stress in smooth rectangular open-channel flows, *J.*
687 *Hydraul. Eng.*, *131,* 30–37.

688 Harris, A. J. L., and S. K. Rowland (2001), FLOWGO: a kinematic thermo-rheological model for
689 lava flowing in a channel, *Bull. Volcanol., 63*, 20–44.

690 Harris, A. J. L., and S. K. Rowland (2009), Effusion rate controls on lava flow length and the
691 role of heat loss: a review, in *Studies in Volcanology: The Legacy of George Walker,* edited by
692 T. Thordarson, S. Self, G. Larsen, S. Rowland, and A. Hoskuldsson, *Spec. Publ. IAVCEI, 2*,
693 33–51.

694 Hon, K., J. Kauahikaua, R. Denlinger, R., and K. Mackay (1994), Emplacement and inflation of
695 pahoehoe sheet flows: Observations and measurements of active lava flows on Kilauea
696 Volcano, Hawaii. *Geol. Soc. Am. Bull., 106* (3), 351–370.

697 James, M. R., H. Pinkerton, and S. Robson (2007), Image-based measurement of flux variation
698 in distal regions of lava flows, *Geochem. Geophys. Geosys., 8(3)*,
699 doi:10.1029/2006GC001448.

James, M.R., H. Pinkerton, M. and Ripepe (2010), Imaging short period variations in lava flux, *Bull. Volcanol., 72*, 671-676, doi: 10.007/s00445-010-0354-y.

Kauahikaua, J., K. V. Cashman, D. A. Clague, D. Champion, J. T. Hagstrum (2002) Emplacement of the most recent lava flows on Hualalai Volcano, Hawaii. *Bull. Volcanol. 64*, 229-253, doi: 10.1007/s00445-001-0196-8.

Keszthelyi, L., S. Self, and T. Thordarson (1999), Application of recent studies on the emplacement of basaltic lava flows to the Deccan Traps. *Memoirs – Geological Society of India, 43*, 485–520.

Mazzarini, F., M. T. Pareschi, M. Favalli, I. Isola, S. Targuini, S., and E. Boschi (2005), Morphology of basaltic lava channels during the Mt. Etna September 2004 eruption from airborne laser altimeter data, *Geophys. Res. Lett*, *32,* L04305, doi: 10.1029/2004GL021815.

McGetchin, T., and J. Eichelberger (1975), Emplacement of the 1801 Hualalai lava flow, Hawaii, *Solid Earth Geosci, Res. Activ. LA-5956-PR,* Los Alamos Natl. Lab., Los Alamos NM.

Mei, C. C. (1966), Nonlinear gravity waves in a thin sheet of viscous fluid, *J. Math. Phys*., *45*, 266–288.

Moore, H. J. (1987), Preliminary estimates of the rheological properties of 1984 Mauna Loa lava, in *Volcanism in Hawaii, U.S. Geol. Surv. Prof. Pap., 1350*, 1569–1588.

Nichols, R. L. (1939), Viscosity of lava, *J. Geol., 41*, 270–302.

Oppenheimer, C. (1991) Lava flow cooling estimated from Landsat Thematic Mapper infrared data: the Lonquimay eruption (Chile, 1989) *J. Geophys. Res. 96 (B13)*, 21,865-21,878.

Rose, S., and M. Ramsey (2009), The 2005 eruption of Kliuchevskoi volcano: Chronology and processes derived from ASTER spaceborne and field-based data, *J. Volcanol. Geotherm. Res.*, *184*, 367-380.

Rowland, S. K., and G. P. L. Walker (1990), Pahoehoe and aa in Hawaii: volumetric flow rate controls the lava structure, *Bull. Volcanol., 52*, 615–628.

Shaw, H.R., and D.A. Swanson, (1970), Eruption and flow rates of flood basalts. In *Proceedings 2nd Columbia River Basalt Symposium*, pp. 271-299, Eastern Washington State College Press, Cheney.

Wright, R., and L. P. Flynn (2003), On the retrieval of lava flow surface temperatures from infrared satellite data, *Geology, 31*, 893–896.

Wright, R., D. A. Rothery, S. Blake, and D. C. Pieri (2000), Improved remote sensing estimates of lava flow cooling: A case study of the 1991 to 1993 Mount Etna eruption, *J. Geophys. Res, 105*, 23,681-23,694.

735 Wright, R., H. Garbeil, and A. G. Davies (2010), Cooling rate of some active lavas determined
736 using an orbital imaging spectrometer, *J. Geophys. Res., 115,* B06205**,** doi:10.1029/2009
737 JB006536.

738

739

Tables

Table 1. Dissipation time constants Γ in seconds for eddy of radius R and viscosity μ.

Eddy radius, R (m)	**Lava dynamic viscosity, μ (Pa s)**			
	10	**100**	**1000**	**10000**
0.5	65	6.5	0.65	0.065
1	260	26	2.6	0.26
2	1040	104	10.4	1.04
5	6500	650	65	6.5
10	26000	2600	260	26

Table 2. Parameters used to calculate lava core cooling

Flow depth, h	5 m
Initial temperature, T_o	1330 K
Lava density, ρ	2600 kg m^{-3}
Lava specific heat, C_p	1225 J kg^{-1} K^{-1}
Lava emissivity, ε	1
Flow velocity, u	0.2 m s^{-1}

Figures

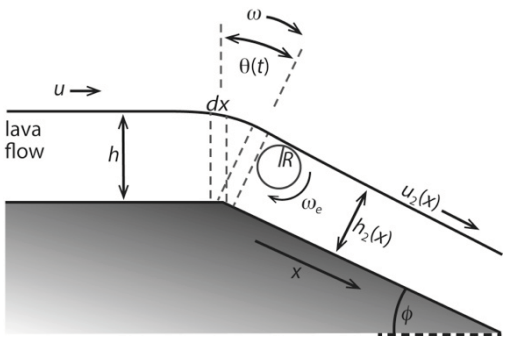

Figure 1. Geometry of a lava flow encountering a slope break. A lava column of height h and thickness dx (dashed lines) rotates through an angle θ with angular velocity ω as it pivots over the slope break, thereby imparting rotational energy to the flow and producing an eddy of radius R and angular velocity ω_e. On the new slope ϕ, the flow takes on new velocity u_2 and depth h_2.

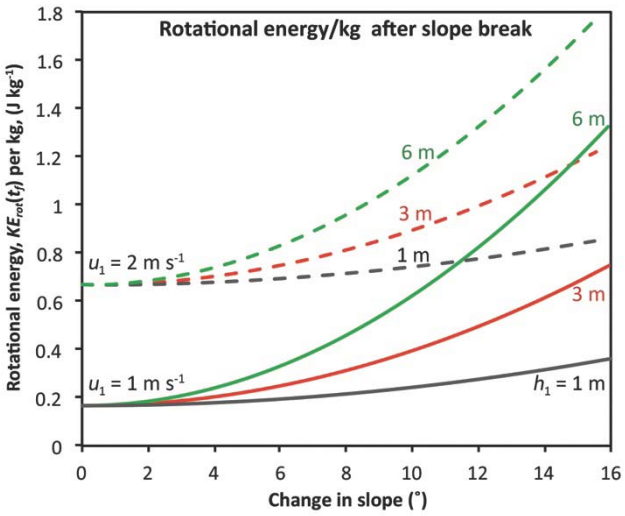

Figure 2. The absolute value of the exit rotational energy $KE_{rot}(t_f)$ per kg as a function of the change in underlying slope at the slope break. The reference case is taken as u_1 = 1 m s^{-1} and h_1 = 1 m for the incident flow. The rotational energy changes by a factor of 2 over slope changes up to 15˚ (solid gray curve). For flows of thickness 3 and 6 m, the rotational energy changes by factors of 4 and 7 (red and green curves), respectively, demonstrating the sensitivity of rotational energy to slope for thicker flows. For comparison, the dashed curves show the effect of a greater incident velocity (u_1 = 2 m s^{-1}): the dependence on slope is essentially the same as for the lower velocity, but there is an overall increase in the rotational energy.

768

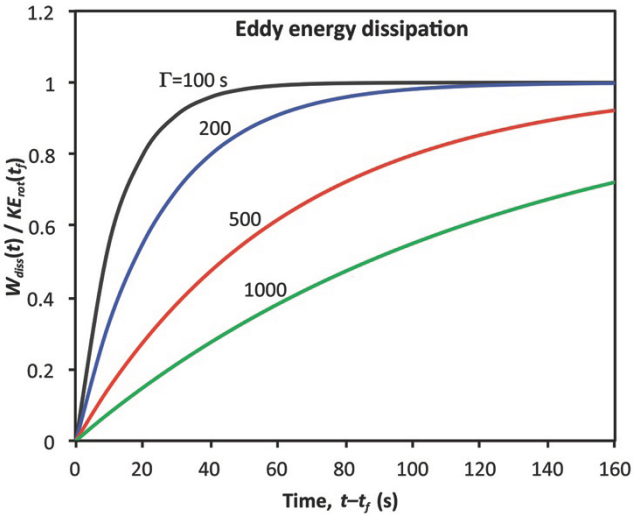

769

770 **Figure 3.** Eddy energy dissipation as a function of time for Γ = 100, 200, 500 and 1000 s from

771 equation (16).

772

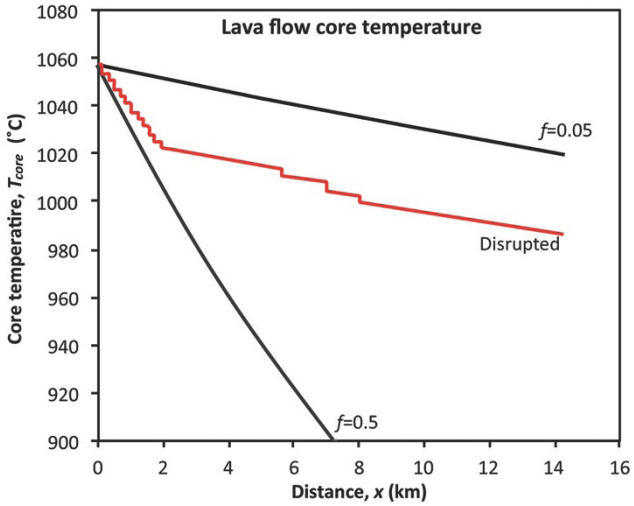

Figure 4. Theoretical temperature profiles along the length of a hypothetical flow for three different values of *f*. The dark curves assume constant core exposure fractions of $f = 0.05$ and $f = 0.5$. For comparison, the red curve shows the strong influence of the T^4 radiation term when the flow surface is disrupted by eddies. Twelve 60 m segments of disruption with $f = 0.9$ were inserted in the first 2 km of the flow, followed by three others further downstream.

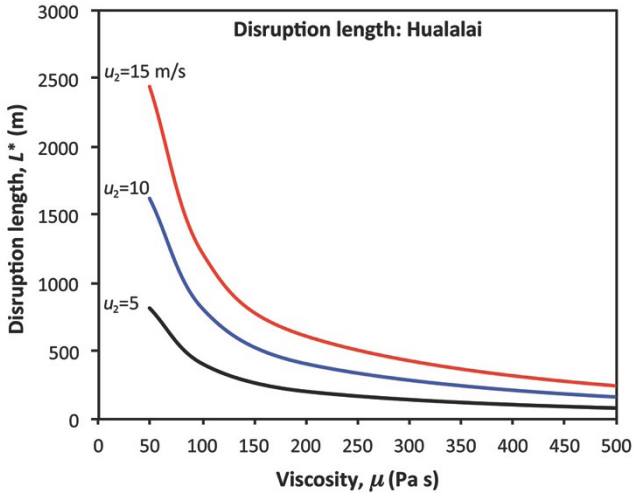

Figure 5. Disruption lengths as a function of viscosity for the lava flow from the 1801 Hualalai eruption for three plausible flow velocities. See text for discussion of parameters.

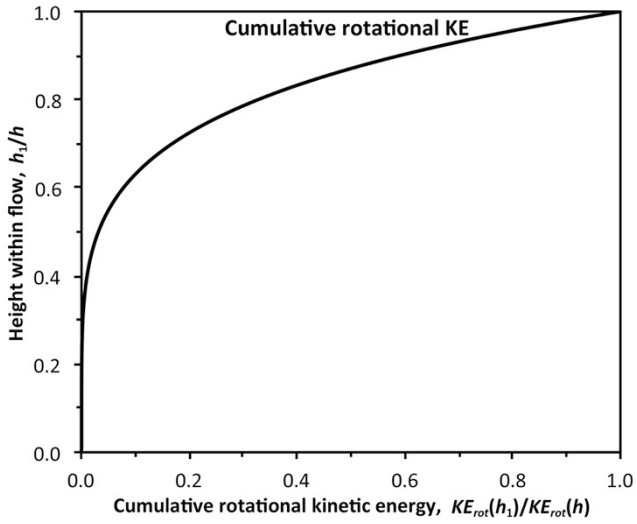

Figure A1. Cumulative rotational kinetic energy for a laminar flow pivoting over an abrupt slope break as a function of the relative depth h_1 within a flow of thickness h.

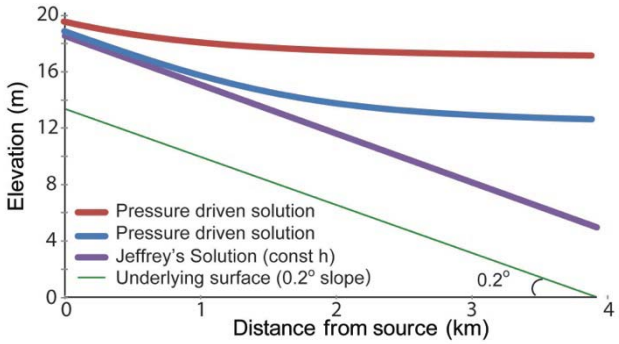

Figure B1. Comparison of steady-state gravity and pressure driven solutions with constant Jeffreys' solution h_J for the flow depth. For clarity of illustration, the slope is taken as 0.2°**.** Once the flow rate, slope and viscosity are fixed, small increases in the flow depth at the source cause a significant departure from the constant Jeffreys' flow depth. At 3–4 km from the source, the flow has more than doubled beyond h_J.